arXiv:1812.01857v1 [cond-mat.supr-con] 5 Dec 2018

Majorana Multipole Response of Topological Superconductors

Shingo Kobayashi,[1,2] Ai Yamakage,[3] Yukio Tanaka,[2] and Masatoshi Sato[4]

[1] *Institute for Advanced Research, Nagoya University, Nagoya 464-8601, Japan*
[2] *Department of Applied Physics, Nagoya University, Nagoya 464-8603, Japan*
[3] *Department of Physics, Nagoya University, Nagoya 464-8602, Japan*
[4] *Yukawa Institute for Theoretical Physics, Kyoto University, Kyoto 606-8502, Japan*

(Dated: February 1, 2022)

In contrast to elementary Majorana particles, emergent Majorana fermions (MFs) in condensed-matter systems may have electromagnetic multipoles. We developed a general theory of magnetic multipoles for surface helical MFs on time-reversal-invariant superconductors. The results show that the multipole response is governed by crystal symmetry, and that a one-to-one correspondence exists between the symmetry of Cooper pairs and the representation of magnetic multipoles under crystal symmetry. The latter property provides a way to identify nonconventional pairing symmetry via the magnetic response of surface MFs. We also find that most helical MFs exhibit a magnetic-dipole response, but those on superconductors with spin-3/2 electrons may display a magnetic-octupole response in leading order, which uniquely characterizes high-spin superconductors. Detection of such an octupole response provides direct evidence of high-spin superconductivity, such as in half-Heusler superconductors.

Introduction. The emergence of Majorana fermions (MFs) in electron systems has led to intense interest in searching for such exotic new excitations in condensed-matter physics. Particularly, recent developments have shown that emergent MFs appear as gapless Andreev bound states in topological superconductors (TSCs) [1–14], which provide a potential candidate for fault-tolerant qubits for topological quantum computation [15]. The increased interest in topological materials has led to a proposal of versatile three-dimensional (3D) time-reversal-invariant (TR-invariant) TSCs, such as superconducting doped topological insulators (TIs) [16–23] and Dirac semimetals [24–29], which commonly host helical MFs forming Kramers pairs on their surfaces.

Emergent MFs share some properties with elementary Majorana particles [30, 31]. For example, both obey Dirac equations with charge-conjugation symmetry. Furthermore, a pair of MF zero modes are required to define the fermionic creation and annihilation operators, from which zero modes exhibit non-Abelian anyon statistics. However, compared with elementary Majorana particles, emergent MFs respond very differently to electric and magnetic fields. Contrarily, neither electric nor magnetic multipoles are possible for elementary MFs [32–34]: $\mathcal{CPT}$ invariance, where $\mathcal{C}$ is charge conjugation, $\mathcal{P}$ is space inversion, and $\mathcal{T}$ is time reversal, is a fundamental symmetry that any relativistic elementary particles is expected to respect. This symmetry forbids intrinsic electric and magnetic multipoles for elementary Majorana particles because they are their own antiparticles under $\mathcal{CPT}$. Contrarily, in superconductors, fundamental symmetry is just charge-conjugation (namely, particle-hole (PH) symmetry), and the emergent MFs are self-conjugate under $\mathcal{C}$. Therefore, MFs in condensed-matter physics are not subject to such a strong constraint, and no systematic study on their electromagnetic multipoles has yet been attempted.

In this Letter, we develop a theory describing the electric and magnetic response of MFs in superconductors. For clarity, we focus here on surface helical MFs on 3D TR-invariant TSCs. A key ingredient specific to emergent MFs is crystalline symmetry. In analogy with $\mathcal{CPT}$ invariance for elementary MFs, crystal symmetry provides additional symmetry constraints on electromagnetic structures of emergent MFs. Considering the constraints, we establish a response theory for helical MFs in a low-energy limit, in which the problem reduces to the selection rule for crystal-symmetry groups. Applying our theory to possible crystal-symmetry groups, we find that helical MFs can host magnetic-multipole structures of dipole or octupole orders as the leading contribution. Additionally, the results predict a one-to-one correspondence between irreducible representation (IR) of Cooper pairs and magnetic multipoles, which helps to determine the pairing symmetry experimentally through the magnetic response of MFs.

Particularly, the proposed theory provides a unique way to identify topological superconductivity of spin-3/2 electrons. Although research interest has recently focused on high-spin topological superconductivity [29, 35–49], little is known about distinguishing TSCs of spin-3/2 electrons from those of spin-1/2 electrons. Thus, we clarify that magnetic responses of helical MFs can unambiguously distinguish between these two types of SCs because the magnetic-octupole response is unique to higher-spin TSCs. To illustrate this, we apply the proposed theory to superconducting TIs of ordinary spin-1/2 electrons [17] and parity-mixed half-Heusler superconductors of spin-3/2 electrons [40, 42]. The results of both numerical and analytical analyses show that only the latter exhibits the octupole response under the same crystalline symmetry.

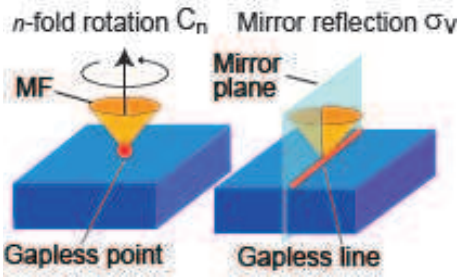


FIG. 1. n-fold rotation and mirror reflection that are compatible with the surface.

Majorana multipole. Helical MFs are a superconducting analogue of surface Dirac fermions of TIs and can be realized in 3D TR-invariant TSCs. From the bulk-boundary correspondence, the existence of helical MFs is ensured by the so-called 3D winding number [4, 5, 50, 51]. Whereas the 3D winding number is defined only for fully gapped TSCs, its parity is well defined even for nodal superconductors [18]. Provided TR symmetry is maintained, these invariants are well defined and protect surface helical MFs for both nodal and nodeless superconductors.

We consider the quantum response of helical MFs when exposed to external electric or magnetic fields. First, note that electric fields only elicit a moderate response from helical MFs because electric fields maintain TR symmetry, helical MFs remains gapless so their response is weak. Conversely, magnetic fields may substantially affect them. Magnetic fields break TR symmetry, so the 3D winding number and its parity become invalid. However, this does not mean that helical MFs are not immune to some magnetic fields because actual TSCs have their own crystalline symmetry. Depending on the direction of the applied magnetic field, TR symmetry may be partially preserved by combining it with crystalline symmetry. Such magnetic crystalline symmetry determines the stability of helical MFs under magnetic fields [52].

As relevant point group operations, we now consider mirror reflections and rotations that are compatible with the surface in question. The mirror plane and the rotation axis should be normal to the surface (see Fig. 1). We consider all two-dimensional point groups formed by them: C_2, C_3, C_4, C_6, C_s, C_{2v}, C_{3v}, C_{4v}, and C_{6v}, in addition to TR symmetry. Under a magnetic field, we retain only magnetic mirror reflection (or magnetic two-fold rotation). Note that the retained magnetic symmetry is selected by the direction of an applied magnetic field: Only for a magnetic field parallel (normal) to the mirror plane (rotation axis) is magnetic mirror reflection (magnetic two-fold rotation) preserved. The above magnetic field is easily seen to flip under TR, but it points back to the original when we simultaneously do a mirror reflection (two-fold rotation).

The retained magnetic symmetry enables TSCs to host an additional topological number that is valid even when the TSC is exposed to a magnetic field. Combining magnetic symmetry with PH symmetry, which is intrinsic to superconductors, one can introduce the magnetic one-dimensional (1D) winding number [53–56]: $w_{\mathrm{M1D}} = \frac{i}{4\pi}\int dk_\perp \mathrm{tr}\left[\Gamma_{\mathrm{M}}\mathcal{H}^{-1}(k_\perp,\boldsymbol{k}_\parallel)\partial_{k_\perp}\mathcal{H}(k_\perp,\boldsymbol{k}_\parallel)\right]$ where $\mathcal{H}(\boldsymbol{k})$ is the Bogoliubov-de Gennes (BdG) Hamiltonian, $(k_\perp,\boldsymbol{k}_\parallel)$ are the momentum normal and parallel to the surface, respectively, and $\Gamma_{\mathrm{M}} \equiv \mathcal{U}\mathcal{T}\mathcal{C}$ is the magnetic chiral operator. Here, $\mathcal{U}$ is a mirror reflection or two-fold rotation. If w_{M1D} for magnetic two-fold rotation (magnetic mirror reflection) is nonzero in the absence of magnetic fields, then helical MFs remain gapless even under a magnetic field normal (parallel) to the rotation axis (mirror plane), provided the system maintains the bulk gap. Conversely, helical MFs do not necessarily remain gapless under other magnetic fields. This direction dependence results in an anisotropic magnetic response of helical MFs. Note that w_{M1D} for magnetic two-fold rotation (magnetic mirror reflection) is defined only on the symmetric axis (plane), so it protects the gapless point (line) of helical MFs at the symmetry axis (plane) in the surface Brillouin zone (see Fig. 1). From the bulk-boundary correspondence, the gapless points or lines are obtained as zero modes $|u_0^{(a)}\rangle$ $(a = 1, 2, \dots)$ of the BdG equation.

To systematically study the magnetic response of MFs, we examine possible contributions of MFs to local operators $\hat{O}(x) = \hat{c}_\sigma^\dagger(x)O_{\sigma,\sigma'}\hat{c}_{\sigma'}(x)$ of electrons, where $\hat{c}_\sigma^\dagger(x)$ and $\hat{c}_\sigma(x)$ are the electron operators and σ is the internal degrees of freedom such as spin, orbital, and so on. To obtain a physical response, the matrix $O_{\sigma,\sigma'}$ should be Hermitian. The MFs have a nonzero response to external fields through local operators $\hat{O}(x)$. For instance, if MFs make a nonzero contribution to the electron-spin operator $\hat{S}_i(x) = \hat{c}_\sigma^\dagger(x)[s_i/2]_{\sigma,\sigma'}\hat{c}_{\sigma'}(x)$ with a Pauli matrix s_i, then the MF shows a nonzero magnetic response through the Zeeman term of electrons.

In the Nambu space with $\hat{\Psi}^\dagger(x) = (\hat{c}_\sigma^\dagger(x), \hat{c}_\sigma(x))$, $\hat{O}(x)$ is recast into $\hat{O}(x) = (1/2)\hat{\Psi}^\dagger(x)\mathcal{O}\hat{\Psi}(x)$, with $\mathcal{O} = \mathrm{diag}(O, -O^T) = \mathrm{diag}(O, -O^*)$, where we have used the Hermiticity of O. Next, by expanding the mode of the quantum field $\hat{\Psi}(x) = \sum_a \hat{\gamma}^{(a)}|u_0^{(a)}\rangle + (\text{nonzero modes})$, we obtain the coupling between $\hat{O}(x)$ and the MFs $\hat{\gamma}^{(a)}$ in the low-energy limit,

$$\begin{aligned}\hat{O}_{\mathrm{MF}} &= \frac{1}{2}\sum_{ab}\hat{\gamma}^{(a)}\hat{\gamma}^{(b)}\langle u_0^{(a)}|\mathcal{O}|u_0^{(b)}\rangle \\ &= -\frac{i}{4}\sum_{ab}\hat{\gamma}^{(a)}\hat{\gamma}^{(b)}\mathrm{tr}\left[\mathcal{O}\rho^{(ab)}\right], \end{aligned} \tag{1}$$

where $\rho^{(ab)} \equiv i\left(|u_0^{(b)}\rangle\langle u_0^{(a)}| - |u_0^{(a)}\rangle\langle u_0^{(b)}|\right)$. In this formalism, crystalline symmetry is properly considered by the irreducible decomposition of $\mathcal{O}$ as $\mathcal{O} = \sum_\Gamma \mathcal{O}_\Gamma$, where $\mathcal{O}_\Gamma$ is an IR of the point group on the surface. As shown

TABLE I. Magnetic multipole of MFs. From left to right, each column shows two-dimensional point groups (PGs), IRs of Δ_Γ with $w_{\mathrm{M1D}} \neq 0$, the basis of Δ_Γ, $\mathcal{U}$ associated with Γ_{M}, IRs of $\mathcal{O}_\Gamma$, and the basis of $\mathcal{O}_\Gamma$. Here, J_i are the spin matrices, "$-$" means the absence of IRs, and $\mathcal{O}_\Gamma$ describes the leading order of the magnetic multipoles.

PG	Δ_Γ	basis of Δ_Γ ($\times e^{-i\pi J_y}$)	$\mathcal{U}$	$\mathcal{O}_\Gamma$	basis of $\mathcal{O}_\Gamma$
C_2, C_4, C_6	A	$\boldsymbol{k}\cdot\boldsymbol{J}$	C_2	A	J_z
C_3	$-$	$-$	$-$	$-$	$-$
C_s	A	$k_xJ_z, k_xJ_y, k_yJ_x, k_zJ_x$	$\sigma_v(yz)$	A	J_x
C_{2v}	A_2	k_zJ_z	C_2	A_2	J_z
	B_1	k_xJ_z, k_zJ_x	$\sigma_v(yz)$	B_1	J_x
	B_2	k_yJ_z, k_zJ_y	$\sigma_v(xz)$	B_2	J_y
C_{3v}	A_1	$k_z(J_x^3 - J_xJ_yJ_y - J_yJ_xJ_y - J_yJ_yJ_x)$	$\sigma_v(yz)$	A_1	$J_x^3 - J_xJ_yJ_y - J_yJ_xJ_y - J_yJ_yJ_x$
C_{4v}	A_2	k_zJ_z	C_2	A_2	J_z
C_{6v}	A_2	k_zJ_z	C_2	A_2	J_z
	B_1	$k_z(J_x^3 - J_xJ_yJ_y - J_yJ_xJ_y - J_yJ_yJ_x)$	$\sigma_v(yz)$	B_1	$J_x^3 - J_xJ_yJ_y - J_yJ_xJ_y - J_yJ_yJ_x$
	B_2	$k_z(J_y^3 - J_yJ_xJ_x - J_xJ_yJ_x - J_xJ_xJ_y)$	$\sigma_d(xz)$	B_2	$J_y^3 - J_yJ_xJ_x - J_xJ_yJ_x - J_xJ_xJ_y$

below, $|u_0^{(a)}\rangle$ obeys several symmetry constraints, so only a few representations of $\mathcal{O}_\Gamma$ can provide nonzero contributions in Eq. (1).

We now discuss the symmetry constraints. First, to have a nonzero w_{M1D}, we need a bulk superconducting gap at the high-symmetry line or plane on which w_{M1D} is defined. This requirement restricts the possible pairing symmetry of Cooper pairs. The pairing symmetry must also maintain TR symmetry because we consider 3D TR-invariant TSCs. Moreover, if the bulk system has inversion symmetry, the pairing symmetry must be odd under inversion [56, 57]. Second, the zero modes $|u_0^{(a)}\rangle$ should be a representation of the point group that is compatible with both the surface and the pairing symmetries because the BdG Hamiltonian respects these symmetries. Note that nonconventional Cooper pairs spontaneously break part of the crystalline symmetry, so the zero modes respect only the unbroken part. Third, a much stronger symmetry constraint is obtained from the index theorem of w_{M1D} [58]. The index theorem says that zero modes $|u_0^{(a)}\rangle$ should be eigenstates of Γ_{M}; for example,

$$\Gamma_{\mathrm{M}}|u_0^{(a)}\rangle = |u_0^{(a)}\rangle. \tag{2}$$

Here all stable zero modes should have the same eigenvalue Γ_{M}, otherwise zero modes with opposite eigenvalues are easily gapped in pairs, even by a symmetry-preserving perturbation. In fact, this important property can be rigorously proven for generic lattice systems [56]. Finally, for the zero modes to exist, any surface-preserving point-group operation for the BdG Hamiltonian should not anticommute with Γ_{M}. The last claim is proven by contradiction. If such a point group operation exists, one can generate another zero mode whose eigenvalue is the opposite of Γ_{M} by operating on a zero mode with the point group. This contradicts the above property of the zero modes, so the claim holds.

Note that the last constraint also restricts any possible pairing symmetry of Cooper pairs. In a nonconventional superconductor, depending on the pairing symmetry, crystalline symmetry can be realized projectively as a combination with a $U(1)$ gauge rotation, which changes their commutation to that of the chiral operator Γ_{M}. For instance, if the gap function (Cooper pair) is odd under a mirror reflection, then the mirror reflection of the BdG Hamiltonian is the original reflection combined with a $U(1)$ π rotation, so it anticommutes with the PH operator. Therefore, its commutation with Γ_{M} changes. As discussed above, stable zero modes only exist when any surface-preserving point-group operation does not anticommute with Γ_{M}, which restricts any possible pairing symmetry between Cooper pairs [57].

Based on these arguments, we determine the possible pairing symmetry of Cooper pairs and IRs of $\rho^{(ab)}$ [57]. We also find that only the same IRs of $\mathcal{O}_\Gamma$ give nonzero contributions in Eq. (1). Table I summarizes the IRs of $\mathcal{O}_\Gamma$ and pairing symmetry that satisfy the above constraints. Remarkably, the results show that the IRs of Δ_Γ and those of $\mathcal{O}_\Gamma$ coincide with each other up to leading order. This notable property allows us to determine the pairing symmetry through the magnetic response of MFs. The results also show that a magnetic-octupole response is possible when the surface has $C_{3\mathrm{v}}$ or $C_{6\mathrm{v}}$ symmetry. As shown below, the octupole response only appears for MFs in high-spin TSCs of spin-3/2 electrons. The order of magnetic multipoles reflects a difference between TSCs with spin 1/2 and 3/2.

Majorana octupole in spin-3/2 superconductors. The results presented in Table I indicate that helical MFs on a surface-preserving C_{3v} or C_{6v} host the magnetic octupole. This unique behavior is intrinsic to high-spin TSCs of spin-3/2 electrons for the following reasons.

First, the base of O_Γ for the magnetic octupole vanishes if the J_i are given by the Pauli matrices of spin-

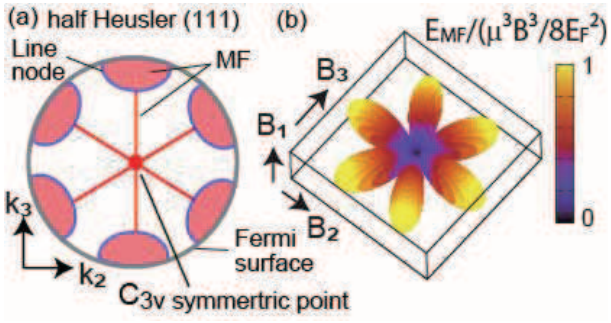


FIG. 2. (a) Surface states of half-Heusler superconductor in (111) plane. The red line and red areas indicate helical MFs with flat dispersion and the line-node-induced Majorana flat bands. $k_1 = \frac{1}{\sqrt{3}}(k_x + k_y + k_z)$, $k_2 = \frac{1}{\sqrt{2}}(k_x - k_y)$, and $k_3 = \frac{1}{\sqrt{6}}(k_x + k_y - 2k_z)$. (b) Energy gap of helical MF at $k_2 = k_3 = 0$ as a function of $\boldsymbol{B}$ under the Zeeman magnetic field $\mu\boldsymbol{B}\cdot\boldsymbol{J}$.

1/2 electrons. In fact, we have $J_x^3 - J_xJ_yJ_y - J_yJ_xJ_y - J_yJ_yJ_x = J_y^3 - J_yJ_xJ_x - J_xJ_yJ_x - J_xJ_xJ_y = 0$ for $J_i = \sigma_i/2$. Furthermore, if the pairing symmetry is A_1 ($B_{i=1,2}$) for C_{3v} (C_{6v}), which is required for the octupole response, the spin-1/2 superconductor hosts a superconducting node at a high-symmetry line, so it cannot support well-defined helical MFs with magnetic octupoles because C_3 symmetry for spin-1/2 electrons is enhanced to C_∞ on the axis of rotation in the Brillouin zone [57].

Contrastingly, for spin-3/2 superconductors, helical MFs exhibit an octupole response. To illustrate this, we calculate the magnetic response of MFs in half-Heusler compounds. In these compounds [35–40], a strong spin-orbit interaction (SOI) and high crystal symmetry provide a fourfold degenerate band at the Γ point, which is well described by spin-3/2 fermions [42]. Additionally, recent experiments have suggested the existence of parity-mixed superconductivity with line nodes [39, 40]. We show here that the parity-mixed superconductor exhibits a magnetic-octupole response. Consider the low-energy model with T_d symmetry [42]:

$$H_{\rm LK}(\boldsymbol{k}) = \alpha\boldsymbol{k}^2 + \beta\sum_i k_i J_i^2 + \gamma\sum_{i\neq j} k_i k_j J_i J_j + \delta\sum_i k_i(J_{i+1}J_iJ_{i+1} - J_{i+2}J_iJ_{i+2}), \quad (3)$$

where $i = x, y, z$ and $i+1 = y$ if $i = x$, etc., and J_i are the 4×4 spin matrices of spin-3/2 fermions. Because inversion symmetry is absent, the Hamiltonian includes the antisymmetric SOI, which is proportional to δ and causes spin splitting at the Fermis surface [40]. In their superconducting states, Cooper pairs form between spin-3/2 electrons, which allows quintet and septet parings in addition to the conventional singlet and triplet pairings [42, 59, 60]. Furthermore, the antisymmetric SOI generally mixes the parity of the gap function, so the even- and odd-parity components coexist in the gap function [61–65] and the odd-parity component is aligned with the antisymmetric SOI [62], providing the spin-septet pairing [40, 42]. Based on this insight, the gap function must include the spin-septet component, $\Delta(\boldsymbol{k}) = \Delta/\sqrt{1+\eta^2}[\eta 1_4 + \sum_i k_i(J_{i+1}J_iJ_{i+1} - J_{i+2}J_iJ_{i+2})](e^{-iJ_y\pi})$, in addition to an s-wave singlet state, even when we choose the conventional A_1 state of T_d, where η parametrizes the mixing between the s-wave and spin-septet components and 1_n is the $n\times n$ identity matrix. Here, the PH, TR, and T_d symmetry operations hosted by the BdG Hamiltonian are $\mathcal{C} = \tau_x K$, $\mathcal{T} = e^{-iJ_y\pi}K$, and $\mathrm{diag}[e^{-i\frac{i2\pi}{q}\boldsymbol{J}\cdot\boldsymbol{n}}, e^{i\frac{i2\pi}{q}\boldsymbol{J}\cdot\boldsymbol{n}}]$, respectively.

The superconducting state hosts six line nodes encircling the k_x, k_y, and k_z axis [42], in analogy with other parity-mixed superconductors [58, 66–71]. Here, we focus on the (111) surface because the magnetic-octupole response requires C_{3v} symmetry. To verify the existence of helical MFs, we numerically diagonalize the BdG Hamiltonian with the surface normal to the [111] direction and find a helical MF with three flat dispersion curves (see Fig. S2 in the Supplemental Material [57]), as schematically depicted in Fig. 2(c). Each flat dispersion curve lies on the mirror planes with mirror-reflection symmetries, σ, $C_3^\dagger\sigma C_3$, and $(C_3^\dagger)^2\sigma(C_3)^2$, where σ is mirror-reflection with respect to the $(1\bar{1}0)$ plane and C_3 is a threefold rotation around the [111] direction. Combining these mirror reflections with PH and TR operations, we obtain three $\Gamma_{\rm M}$ and the associated $w_{\rm M1D}$, which protects zero modes on each flat dispersion curve. In particular, the three flat dispersion curves meet at a C_{3v} symmetry point.

Based on the constraint (2), the zero modes can be simultaneous eigenstates of $\Gamma_{\rm M}$ and of C_3. In this case, we have $\Gamma_{\rm M}|u_0^{(a)}\rangle = |u_0^{(a)}\rangle$ and $C_3|u_0^{(a)}\rangle = -|u_0^{(a)}\rangle$ with $a = 1, 2$ being the label for a Kramers pair [57], which lead to $\Gamma_{\rm M}\rho^{(12)}\Gamma_{\rm M}^{-1} = C_3\rho^{(12)}C_3^{-1} = \rho^{(12)}$. Thus, $\mathcal{O}_\Gamma$ needs to be the trivial representation A_1 in C_{3v}, as shown in Table I. To demonstrate magnetic response, we add a Zeeman magnetic term $\mu\boldsymbol{B}\cdot\boldsymbol{J}$ in Eq. (3), which leads to an anisotropic response with C_3 symmetry in Fig. 2(d). The Zeeman magnetic term contributes to the energy gap of the MFs on the order of $3\sqrt{2}\mu^3B^3/32E_F^2$, where E_F is the Fermi energy [57], implying a magnetic-octupole response.

Another high-spin superconductor of spin-3/2 electrons was recently proposed for antiperovskite materials with O_h group [28, 29]. We obtain a similar magnetic-octupole response of MFs on the (111) surface when its pairing symmetry is A_{2u} of O_h.

For comparison, we also examine magnetic response of helical MFs in the doped superconducting TI, $A_x{\rm Bi_2Se_3}$ (A=Cu, Sr, Nb), which becomes a TSC when an odd-parity Cooper pair is realized [5, 17, 21–23, 51]. Since $\rm Bi_2Se_3$ has D_{3d} symmetry, the surface normal to the c axis (i.e., (111) surface) hosts C_{3v} symmetry like the half-

Heusler case. However, the doped TI merely exhibits the magnetic-dipole response of MFs to leading order, or it cannot host a well-define helical MFs on the (111) surface [57, 72], since it is a conventional spin-1/2 TSC.

Conclusions. In this paper, we develop a theory of Majorana multipoles for 3D TR-invariant TSCs, which provide novel experimental means to identify bulk pairing symmetry and high-spin superconductivity. The Majorana multipoles may be observed through spin-sensitive measurements such as spatially resolved NMR measurements [73] or the surface tunneling spectroscopy under magnetic fields [74–79].

This work was supported by the Grants-in-Aid for Scientific Research on Innovative Areas "Topological Material Science" (Grant Nos. JP15H05855, JP15H05851, JP15H05853, JP15K21717, and JP18H04224) from JSPS of Japan, and by JSPS KAKENHI Grant Nos. JP17H02922 and JP18H01176. S.K. was supported by the CREST project (JPMJCR16F2) from Japan Science and Technology Agency (JST), and the Building of Consortia for the Development of Human Resources in Science and Technology.

[1] C.-R. Hu, Phys. Rev. Lett. **72**, 1526 (1994).
[2] S. Kashiwaya and Y. Tanaka, Rep. Prog. Phys. **63**, 1641 (2000).
[3] G. E. Volovik, *The Universe in a Helium Droplet* (Oxford University Press, Oxford, 2003).
[4] A. P. Schnyder, S. Ryu, A. Furusaki, and A. W. W. Ludwig, Phys. Rev. B **78**, 195125 (2008).
[5] M. Sato, Phys. Rev. B **79**, 214526 (2009).
[6] F. Wilczek, Nature Phys. **5**, 614 (2009).
[7] M. Z. Hasan and C. L. Kane, Rev. Mod. Phys. **82**, 3045 (2010).
[8] X.-L. Qi and S.-C. Zhang, Rev. Mod. Phys. **83**, 1057 (2011).
[9] Y. Tanaka, M. Sato, and N. Nagaosa, Journal of the Physical Society of Japan **81**, 011013 (2012).
[10] J. Alicea, Rep. Prog. Phys. **75**, 076501 (2012).
[11] M. Sato and S. Fujimoto, Journal of the Physical Society of Japan **85**, 072001 (2016).
[12] T. Mizushima, Y. Tsutsumi, T. Kawakami, M. Sato, M. Ichioka, and K. Machida, Journal of the Physical Society of Japan **85**, 022001 (2016).
[13] C.-K. Chiu, J. C. Y. Teo, A. P. Schnyder, and S. Ryu, Rev. Mod. Phys. **88**, 035005 (2016).
[14] M. Sato and Y. Ando, Rep. Prog. Phys. **80**, 076501 (2017).
[15] C. Nayak, S. H. Simon, A. Stern, M. Freedman, and S. Das Sarma, Rev. Mod. Phys. **80**, 1083 (2008).
[16] Y. S. Hor, A. J. Williams, J. G. Checkelsky, P. Roushan, J. Seo, Q. Xu, H. W. Zandbergen, A. Yazdani, N. P. Ong, and R. J. Cava, Phys. Rev. Lett. **104**, 057001 (2010).
[17] L. Fu and E. Berg, Phys. Rev. Lett. **105**, 097001 (2010).
[18] S. Sasaki, M. Kriener, K. Segawa, K. Yada, Y. Tanaka, M. Sato, and Y. Ando, Phys. Rev. Lett. **107**, 217001 (2011).
[19] S. Sasaki, Z. Ren, A. A. Taskin, K. Segawa, L. Fu, and Y. Ando, Phys. Rev. Lett. **109**, 217004 (2012).
[20] T. Hashimoto, K. Yada, M. Sato, and Y. Tanaka, Phys. Rev. B **92**, 174527 (2015).
[21] L. Fu, Phys. Rev. B **90**, 100509 (2014).
[22] K. Matano, M. Kriener, K. Segawa, Y. Ando, and G.-q. Zheng, Nature Physics **12**, 852 (2016).
[23] S. Yonezawa, K. Tajiri, S. Nakata, Y. Nagai, Z. Wang, K. Segawa, Y. Ando, and Y. Maeno, Nature Physics **13**, 123 (2016).
[24] L. Aggarwal, A. Gaurav, G. S. Thakur, Z. Haque, A. K. Ganguli, and G. Sheet, Nature Materials **16**, 3237 (2015).
[25] H. Wang, H. Wang, H. Liu, H. Lu, W. Yang, S. Jia, X.-J. Liu, X. C. Xie, J. Wei, and J. Wang, Nature Materials **15**, 3842 (2015).
[26] S. Kobayashi and M. Sato, Phys. Rev. Lett. **115**, 187001 (2015).
[27] T. Hashimoto, S. Kobayashi, Y. Tanaka, and M. Sato, Phys. Rev. B **94**, 014510 (2016).
[28] M. Oudah, A. Ikeda, J. N. Hausmann, S. Yonezawa, T. Fukumoto, S. Kobayashi, M. Sato, and Y. Maeno, Nature Communications **7**, 13617 (2016).
[29] T. Kawakami, T. Okamura, S. Kobayashi, and M. Sato, Phys. Rev. X **8**, 041026 (2018).
[30] E. Majorana, Nuovo Cimento **14**, 171 (1937).
[31] F. T. Avignone, S. R. Elliott, and J. Engel, Rev. Mod. Phys. **80**, 481 (2008).
[32] B. Kayser and A. S. Goldhaber, Phys. Rev. D **28**, 2341 (1983).
[33] E. E. Radescu, Phys. Rev. D **32**, 1266 (1985).
[34] F. Boudjema, C. Hamzaoui, V. Rahal, and H. C. Ren, Phys. Rev. Lett. **62**, 852 (1989).
[35] G. Goll, M. Marz, A. Hamann, T. Tomanic, K. Grube, T. Yoshino, and T. Takabatake, Physica B: Condensed Matter **403**, 1065 (2008).
[36] N. P. Butch, P. Syers, K. Kirshenbaum, A. P. Hope, and J. Paglione, Phys. Rev. B **84**, 220504 (2011).
[37] F. F. Tafti, T. Fujii, A. Juneau-Fecteau, S. René de Cotret, N. Doiron-Leyraud, A. Asamitsu, and L. Taillefer, Phys. Rev. B **87**, 184504 (2013).
[38] G. Xu, W. Wang, X. Zhang, Y. Du, E. Liu, S. Wang, G. Wu, Z. Liu, and X. X. Zhang, Scientific Reports **4**, 5709 (2014).
[39] T. V. Bay, T. Naka, Y. K. Huang, and A. de Visser, Phys. Rev. B **86**, 064515 (2012).
[40] H. Kim, K. Wang, Y. Nakajima, R. Hu, S. Ziemak, P. Syers, L. Wang, H. Hodovanets, J. D. Denlinger, P. M. R. Brydon, D. F. Agterberg, M. A. Tanatar, R. Prozorov, and J. Paglione, Science Advances **4**, eaao4513 (2018).
[41] I. Boettcher and I. F. Herbut, Phys. Rev. B **93**, 205138 (2016).
[42] P. M. R. Brydon, L. Wang, M. Weinert, and D. F. Agterberg, Phys. Rev. Lett. **116**, 177001 (2016).
[43] L. Savary, J. Ruhman, J. W. F. Venderbos, L. Fu, and P. A. Lee, Phys. Rev. B **96**, 214514 (2017).
[44] B. Roy, S. A. A. Ghorashi, M. S. Foster, and A. H. Nevidomskyy, ArXiv e-prints (2017), arXiv:1708.07825 [cond-mat.mes-hall].
[45] C. Timm, A. P. Schnyder, D. F. Agterberg, and P. M. R. Brydon, Phys. Rev. B **96**, 094526 (2017).
[46] J. W. F. Venderbos, L. Savary, J. Ruhman, P. A. Lee, and L. Fu, Phys. Rev. X **8**, 011029 (2018).

[47] I. Boettcher and I. F. Herbut, Phys. Rev. Lett. **120**, 057002 (2018).
[48] J. Yu and C.-X. Liu, ArXiv e-prints (2018), arXiv:1801.00083 [cond-mat.supr-con].
[49] I. Kuzmenko, T. Kuzmenko, Y. Avishai, and M. Sato, Phys. Rev. B **98**, 165139 (2018).
[50] P. G. Grinevich and G. E. Volovik, Journal of Low Temperature Physics **72**, 371 (1988).
[51] M. Sato, Phys. Rev. B **81**, 220504 (2010).
[52] These relations lead to $\{\mathcal{C}, \rho^{(12)}\} = \{\mathcal{T}, \rho^{(12)}\} = 0$, which are consistent with $\{\mathcal{C}, \mathcal{O}_\Gamma\} = \{\mathcal{T}, \mathcal{O}_\Gamma\} = 0$.
[53] T. Mizushima, M. Sato, and K. Machida, Phys. Rev. Lett. **109**, 165301 (2012).
[54] K. Shiozaki and M. Sato, Phys. Rev. B **90**, 165114 (2014).
[55] E. Dumitrescu, J. D. Sau, and S. Tewari, Phys. Rev. B **90**, 245438 (2014).
[56] Y. Xiong, A. Yamakage, S. Kobayashi, M. Sato, and Y. Tanaka, Crystals **7**, 58 (2017).
[57] See the Supplemental Material at [URL will be inserted by publisher] for the detail calculation.
[58] M. Sato, Y. Tanaka, K. Yada, and T. Yokoyama, Phys. Rev. B **83**, 224511 (2011).
[59] T.-L. Ho and S. Yip, Phys. Rev. Lett. **82**, 247 (1999).
[60] W. Yang, Y. Li, and C. Wu, Phys. Rev. Lett. **117**, 075301 (2016).
[61] L. P. Gor'kov and E. I. Rashba, Phys. Rev. Lett. **87**, 037004 (2001).
[62] P. A. Frigeri, D. F. Agterberg, A. Koga, and M. Sigrist, Phys. Rev. Lett. **92**, 097001 (2004).
[63] S. Fujimoto, Journal of the Physical Society of Japan **76**, 034712 (2007).
[64] S. Fujimoto, Journal of the Physical Society of Japan **76**, 051008 (2007).
[65] E. Bauer, M. Sigrist, and editors, *Non-Centrosymmetric Superconductors: Introduction and Overview* (Springer, Heidelberg, 2012).
[66] Y. Tanaka, Y. Mizuno, T. Yokoyama, K. Yada, and M. Sato, Phys. Rev. Lett. **105**, 097002 (2010).
[67] K. Yada, M. Sato, Y. Tanaka, and T. Yokoyama, Phys. Rev. B **83**, 064505 (2011).
[68] P. M. R. Brydon, A. P. Schnyder, and C. Timm, Phys. Rev. B **84**, 020501 (2011).
[69] A. P. Schnyder, P. M. R. Brydon, and C. Timm, Phys. Rev. B **85**, 024522 (2012).
[70] S. Matsuura, P.-Y. Chang, A. P. Schnyder, and S. Ryu, New Journal of Physics **15**, 065001 (2013).
[71] A. P. Schnyder and P. M. R. Brydon, Journal of Physics: Condensed Matter **27**, 243201 (2015).
[72] S. Sumita and Y. Yanase, Phys. Rev. B **97**, 134512 (2018).
[73] S. B. Chung and S.-C. Zhang, Phys. Rev. Lett. **103**, 235301 (2009).
[74] M. Fogelström, D. Rainer, and J. A. Sauls, Phys. Rev. Lett. **79**, 281 (1997).
[75] Y. Tanaka and S. Kashiwaya, Phys. Rev. Lett. **74**, 3451 (1995).
[76] Y. Tanaka, Y. Tanuma, K. Kuroki, and S. Kashiwaya, Journal of the Physical Society of Japan **71**, 2102 (2002).
[77] Y. Tanuma, K. Kuroki, Y. Tanaka, R. Arita, S. Kashiwaya, and H. Aoki, Phys. Rev. B **66**, 094507 (2002).
[78] Y. Tanaka, T. Yokoyama, A. V. Balatsky, and N. Nagaosa, Phys. Rev. B **79**, 060505 (2009).
[79] S. Tamura, S. Kobayashi, L. Bo, and Y. Tanaka, Phys. Rev. B **95**, 104511 (2017).

Supplemental Materials: Majorana multipole response of topological superconductors

S1. Symmetry constraints on gap functions and $\mathcal{O}_\Gamma$'s

Here we discuss general symmetry constraints on helical Majorana fermions (MFs) appearing on a surface Brillouin zone (BZ) of time-reversal (TR) invariant topological superconductors (TSCs). As relevant point group symmetry, we consider mirror reflections and rotations that are compatible to the surface. We take into account all 2D point groups formed by them, $C_2, C_3, C_4, C_6, C_s, C_{2v}, C_{3v}, C_{4v}, C_{6v}$ in addition to TR symmetry. These symmetries should be manifest in the Bogoliubov-de Gennes (BdG) Hamiltonian. In the case of nematic superconductors, where a part of crystalline symmetry is spontaneously broken, we consider only the unbroken part.

As is discussed in the main text, helical MFs show anisotropic behaviors under magnetic fields. These behaviors are governed by two different magnetic point group symmetries, magnetic two-fold rotation and magnetic mirror reflection. In what follows, for the sake of concreteness, we consider the case where helical MFs are protected by magnetic twofold rotation symmetry. The case where helical MFs are protected by magnetic mirror-reflection symmetry can be discussed in a similar fashion.

First, we consider symmetry constraints on gap functions. As pairing symmetry, we only need to take into account one-dimensional (1D) irreducible representations (IRs): In general, if a gap function belongs to a higher dimensional IR, it spontaneously breaks crystalline symmetry and/or TR symmetry. In the former case, we should consider the unbroken part of crystalline symmetry, where the gap function belongs to a 1D IR. Furthermore, the latter case is excluded since we consider TR-invariant TSCs. Thus, we have the following constraint,

(a) The gap function is a 1D IR.

Additional constraints are required to obtain a nonzero w_{M1D}. Consider the 1D winding number w_{M1D} with respect to two-fold rotation C_2,

$$w_{M1D} = \frac{i}{4\pi} \int dk_\perp \mathrm{tr} \left[\Gamma_{\mathrm{M}} \mathcal{H}^{-1}(k_\perp, \boldsymbol{k}_\parallel) \partial_{k_\perp} \mathcal{H}(k_\perp, \boldsymbol{k}_\parallel) \right], \tag{S.1}$$

where $\mathcal{H}(\boldsymbol{k})$ is the BdG Hamiltonian, $(k_\perp, \boldsymbol{k}_\parallel)$ are momenta normal and parallel to the surface, and $\Gamma_{\rm M} \equiv e^{i\alpha} C_2 \mathcal{T}\mathcal{C}$ is the magnetic chiral operator with respect to magnetic two-fold rotation. Here we choose α so as $\Gamma_{\rm M}^2 = 1$. When the gap function is even (odd) under two-fold rotation, the two-fold rotation operator C_2 for the BdG Hamiltonian satisfies $[\mathcal{C}, C_2] = 0$ ($\{\mathcal{C}, C_2\} = 0$). For $w_{\rm M1D}$ to be nonzero, however, C_2 should satisfy $[\mathcal{C}, C_2] = 0$. Actually, when $\{\mathcal{C}, C_2\} = 0$, $\Gamma_{\rm M}$ with $\Gamma_{\rm M}^2 = 1$ is given as $\Gamma_{\rm M} = iC_2\mathcal{T}\mathcal{C}$, which leads to $\{\mathcal{T}, \Gamma_{\rm M}\} = 0$. Then, when $\{\mathcal{T}, \Gamma_{\rm M}\} = 0$, the magnetic 1D winding number should be zero [56]. Thus, we have the following constraint,

(b) The gap function is even under two-fold rotation.

Furthermore, when mirror-reflection symmetry σ coexists, we obtain the following:

(c) The gap function is odd under mirror reflection.

This is because $w_{\rm M1D} = 0$ if the gap function is even under mirror reflection. When the gap function is even under reflection, it holds that $[\sigma, \mathcal{C}] = 0$. Therefore, from $[\mathcal{T}, \sigma] = \{C_2, \sigma\} = 0$, we obtain $\{\sigma, \Gamma_{\rm M}\} = 0$, which yields $w_{\rm M1D} = 0$ [56]. Using the conditions (a), (b), (c), and (b)' explained later, we can determine IRs of gap functions as shown in Table I in the main text. We note that if inversion symmetry $\mathcal{I}$ exists in the bulk superconductor, the magnetic 1D winding number is nonzero only when $\{\Gamma_{\rm M}, \mathcal{I}\} = 0$ [56], which leads to $\{\mathcal{I}, \mathcal{C}\} = 0$. The commutation relation implies that the gap function is odd under inversion which is consistent with the condition for obtaining nontrivial TSCs [5, 17, 51].

Next, we discuss symmetry constraints on $\mathcal{O}_\Gamma$'s. From the index theorem, a wave function of MFs at the zero energy $|u_0^{(a)}\rangle$ satisfies

$$\Gamma_{\rm M}|u_0^{(a)}\rangle = |u_0^{(a)}\rangle, \tag{S.2}$$

where $\Gamma_{\rm M} = C_2\mathcal{T}\mathcal{C}$. Hence, we obtain $\Gamma_{\rm M}\rho^{(ab)}\Gamma_{\rm M}^\dagger = \rho^{(ab)}$, where $\rho^{(ab)} \equiv i(|u_0^{(a)}\rangle\langle u_0^{(b)}| - |u_0^{(b)}\rangle\langle u_0^{(a)}|)$. In order for the multipole response to exist, IRs of $\mathcal{O}_\Gamma$ need coincide with IRs of $\rho^{(ab)}$. So, $\mathcal{O}_\Gamma$ should satisfy

$$\Gamma_{\rm M}\mathcal{O}_\Gamma\Gamma_{\rm M}^\dagger = \mathcal{O}_\Gamma. \tag{S.3}$$

From the definition, we have $\{\mathcal{C}, \mathcal{O}_\Gamma\} = 0$. Then, for magnetic responses, $\mathcal{O}_\Gamma$ should be odd under TR, i.e.$\{\mathcal{T}, \mathcal{O}_\Gamma\} = 0$. Thus, we obtain

$$C_2\mathcal{O}_\Gamma C_2^\dagger = \mathcal{O}_\Gamma, \tag{S.4}$$

which implies the following the constraint:

(d) $\mathcal{O}_\Gamma$ is a 1D IR with $C_2 = 1$.

Now, we take into account mirror-reflection symmetry. The constraint (c) implies that $\{\mathcal{C}, \sigma\} = 0$, and by combining it with $[\mathcal{T}, \sigma] = \{C_2, \sigma\} = 0$, we obtain $[\Gamma_{\rm M}, \sigma] = 0$. Therefore, MFs at the zero energy $|u_0^{(a)}\rangle$ can be simultaneous eigenstates of $\Gamma_{\rm M}$ and σ. For a Kramers pair of MFs $|u_0^{(a)}\rangle$ $(a = 1, 2)$, we place the relations

$$\mathcal{C}|u_0^{(a)}\rangle = |u_0^{(a)}\rangle, \quad (a = 1, 2), \tag{S.5}$$

$$\mathcal{T}|u_0^{(1)}\rangle = |u_0^{(2)}\rangle, \tag{S.6}$$

without loss of generality [**?**]. Then, from $[\mathcal{T}, \sigma] = 0$, we have

$$\sigma|u_0^{(a)}\rangle = (-)^a i|u_0^{(a)}\rangle, \quad (a = 1, 2). \tag{S.7}$$

in addition to Eq.(S.2). Equation (S.7) leads to $\sigma\rho^{(12)}\sigma^{-1} = -\rho^{(12)}$, implying that

$$\sigma\mathcal{O}_\Gamma\sigma^{-1} = -\mathcal{O}_\Gamma. \tag{S.8}$$

Thus, we find the following constraint:

(e) $\mathcal{O}_\Gamma$ is a 1D IR with $\sigma = -1$.

When there are multiple Kramers pairs of MFs, $\rho^{(ab)}$ can contain other IRs which behave differently from Eq.(S.8). But we find that the other IRs only gives a subleading contribution for magnetic responses.

Finally, we discuss the action of C_n ($n \geq 3$) on $\mathcal{O}_\Gamma$. From the constraint (a), C_n may have two possible commutation relations with $\mathcal{C}$: When the gap function is even (odd) under C_n, then we have $[C_n, \mathcal{C}] = 0$ ($\{C_n, \mathcal{C}\} = 0$). However, stable helical MFs protected by magnetic two fold rotation are possible only when $[C_n, \mathcal{C}] = 0$: When $\{C_n, \mathcal{C}\} = 0$, it holds that $\{\Gamma_{\rm M}, C_n\} = 0$, and thus $C_n|u_0^{(a)}\rangle$ and $|u_0^{(a)}\rangle$ have opposite chirailties with respect to $\Gamma_{\rm M}$. As a result, they can be easily gapped out without topological protection. Therefore, we have the following constraint

(b)' The gap function is even under C_n,

which includes the constraint (b) as a special case. When the constraint (b)' is satisfied, we have $[\mathcal{C}, C_n] = 0$, and thus from $[C_n, \mathcal{T}] = [C_2, C_n] = 0$, we can show that $[\Gamma_{\rm M}, C_n] = 0$. Therefore, $|u_0^{(a)}\rangle$ is a simultaneous eigenstate of $\Gamma_{\rm M}$ and C_n,

$$C_n|u_0^{(a)}\rangle = \lambda^{(a)}|u_0^{(a)}\rangle, \tag{S.9}$$

where $\lambda^{(a)}$ is an eigenvalue of C_n. For a Kramer pair of MFs $|u_n^{(a)}\rangle$ ($a = 1, 2$), we also have Eqs. (S.5) and (S.6), which lead to $\lambda^{(1)} = \lambda^{(2)} = 1$. Therefore, we obtain $C_n\rho^{(12)}C_n^{-1} = \rho^{(12)}$, implying that

$$C_n\mathcal{O}_\Gamma C_n^\dagger = \mathcal{O}_\Gamma. \tag{S.10}$$

Thus, we find the following constraint:

(d)' $\mathcal{O}_\Gamma$ is a 1D IR with $C_n = 1$,

which include (d) as a special case. Again, when there are multiple Kramers pairs of MFs, $\rho^{(ab)}$ can contain other IRs which behave differently from Eq.(S.10) with $n \geq 3$, but they only gives a subleading contribution for magnetic responses.

Using the constraints (d)' and (e), we can determine IRs of $\mathcal{O}_\Gamma$'s with the leading contributions in Table I in the main text. Note that subleading contributions may exist when there are more than two Kramers pairs of MFs, which do not necessarily satisfy the constraints (e) and (d)' with $n \geq 3$.

S2. Magnetic response of superconducting topological insulators

As is shown in the main text, helical MFs in spin-3/2 superconductors show the magnetic octupole response on a surface preserving $C_{3\rm v}$ symmetry. Here we examine magnetic responses of MFs in spin-1/2 superconductors on a surface with the same symmetry. In contrast to the spin-3/2 case, we find that MFs in spin-1/2 superconductors do not show the magnetic octupole response in the leading order.

Here we consider the superconducting doped topological insulator (TI), $A_x{\rm Bi}_2{\rm Se}_3$ (A=Cu, Sr, Nb), as a representative example of spin-1/2 superconductors. The crystal point group is D_{3d}, and thus a surface perpendicular to the c-axis hosts $C_{3\rm v}$ symmetry. The system consists of two bands near the Fermi energy, which are predominated by Se p_z orbitals on the top and bottom layer of the unit cell. These orbital degrees of freedom do not provide any non-trivial contribution under rotation around the c-axis, and thus these bands behave as ordinary spin-1/2 electrons under C_{3v}.

The low-energy Hamiltonian in the normal state is given by [17]

$$H_{\rm TI}(\boldsymbol{k}) = c(\boldsymbol{k}) + m(\boldsymbol{k})\sigma_x + v_z k_z\sigma_y + v(k_x s_y - k_y s_x)\sigma_z + \lambda(k_x^3 - 3k_x k_y^2)s_z, \tag{S.11}$$

with $c(\boldsymbol{k}) = c_0 + c_1 k_z^2 + c_1(k_x^2 + k_y^2)$ and $m(\boldsymbol{k}) = m_0 + m_1 k_z^2 + m_1(k_x^2 + k_y^2)$. Here σ_i and s_i are the Pauli matrices in the orbital and spin spaces, respectively. The last term proportional to λ is the hexagonal warping term. The symmetries in Eq. (S.11) are TR symmetry $T = is_yK$, inversion symmetry $I = \sigma_x$, three-fold rotation around the c axis $C_3 = e^{-i\frac{\pi}{3}s_z}$, and the vertical mirror reflection $\sigma_v(yz) = is_x$ with respect to the yz plane. Importantly, at the $k_x = k_y = 0$, where Eq. (S.11) is reduced to $H_{\rm TI}(0, 0, k_z) = c(0, 0, k_z) + m(0, 0, k_z)\sigma_z$, the three-fold rotation symmetry becomes fully rotational invariance with $C_\infty = e^{i\frac{s_z}{2}\theta}$ ($0 \leq \theta < 2\pi$). As we shall explained in S3, this symmetry enhancement is intrinsic to spin-1/2 systems.

In superconducting states, the BdG Hamiltonian is given by

$$\mathcal{H}_{\rm TI}(\boldsymbol{k}) = \begin{pmatrix} H_{\rm TI}(\boldsymbol{k}) - \mu & \Delta(\boldsymbol{k}) \\ \Delta(\boldsymbol{k})^\dagger & -H_{\rm TI}(-\boldsymbol{k})^t + \mu \end{pmatrix}, \tag{S.12}$$

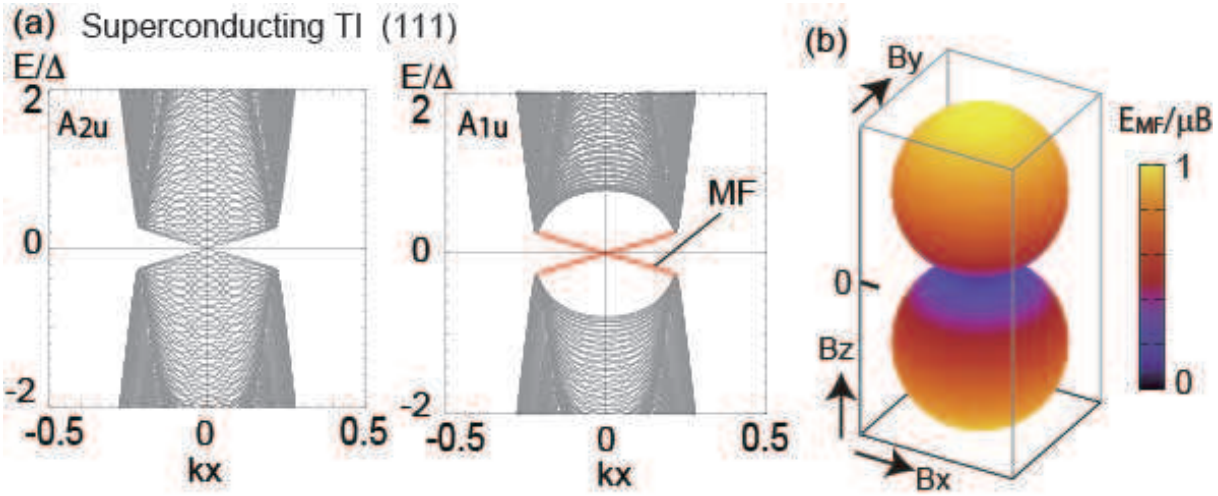


FIG. S1. (a) Surface energy spectrum of Eq. (S.11) at the (111) plane, where we replace k_i, k_i^2 with $\sin k_i$, $2(1-\cos k_i)$ and the (111) plane is perpendicular to c axis. $(c_0, c_1, c_2, m_0, m_1, m_2, v_z, v, \mu, \Delta) = (-0.0083, 5.74, 30.4, -0.28, 6.84, 44.5, 3.33, 2.26, 3, 1)$ (b) Energy gap of the helical MF at $k_x = k_y = 0$ in the superconducting TI with the A_{1u} gap function.

where μ is the chemical potential and $\Delta(\boldsymbol{k})$ is the gap function. Due to the Fermi statistics, we have six on-site gap functions: $(\Delta_0 i s_y, \Delta_0 i\sigma_x s_y, \Delta_0 i\sigma_z s_y, \Delta_0 \sigma_y s_z, \Delta_0 i\sigma_y, \Delta_0 \sigma_y s_x)$, which are classified within D_{3d} such that $(A_{1g}, A_{1g}, A_{2u}, E_u, E_u, A_{1u})$. It has been known that the A_{1u} gap function realizes full-gap TSC [17] and the E_u gap function the nematic superconductor [21–23]. Here we examine magnetic responses for the A_{2u} and A_{1u} gap functions.

First, we consider the A_{2u} gap function, which belongs to A_1 in C_{3v} at the surface BZ. Although the spin-3/2 case with the same pairing symmetry hosts MFs with a magnetic octupole response, the present case do not. As is shown in Fig. S1 (a), there appear point nodes on the C_{3v} symmetric line, so no clear MFs is obtained. This is due to the spin-1/2 nature of the system. As C_3 is enhanced to C_∞ on the k_z-axis, the A_{2u} pairing symmetry cannot support a nonzero gap on the k_z-axis. (See also the group theoretical analysis in [72].)

In the case of the A_{1u} gap function, we have a helical MF on a surface normal to the c-axis. See Fig. S1 (a). Applying the magnetic Zeeman field $\mu \boldsymbol{B} \cdot \boldsymbol{s}$, we calculate the energy gap of the helical MF. As illustrated in Fig. S1 (b), the energy gap results in the dipole response with respect to the c-axis. Again, this behavior is due to the spin-1/2 nature of the system: Because of the enhanced rotation symmetry C_∞, we can define the magnetic 1D winding number by using C_2 subgroup of C_∞. The magnetic winding number is nonzero, and thus the helical MF remains gapless as long as one keeps the magnetic symmetry of C_2. The magnetic symmetry is broken under a magnetic field with a nonzero component along the c-axis, so we have the magnetic dipole response.

S3. Enhancement of rotational symmetry in spin-1/2 systems

We discuss here that the enhancement of rotational symmetry is specific to spin-1/2 systems. We start from an effective Hamiltonian with basis $|\pm j_z\rangle$, which is generally described by

$$H(\boldsymbol{k}) = a_0(\boldsymbol{k}) s_0 + a_x(\boldsymbol{k}) s_x + a_y(\boldsymbol{k}) s_y + a_z(\boldsymbol{k}) s_z, \tag{S.13}$$

where s_i are the Pauli matrices with basis $|\pm j_z\rangle$ and $a_i(\boldsymbol{k})$ are real functions of $\boldsymbol{k}$. We are interested in the behavior of the Hamiltonian on a high symmetric axis where the enhancement of rotational symmetry may occur. Hereafter, we focus on a $C_{3\mathrm{v}}$ symmetric axis, say k_z axis. Practically, there exists a $C_{3\mathrm{v}}$ symmetric axis along the [111] direction in the superconducting TIs and half-Heusler superconductors. On the k_z line, the Hamiltonian (S.13) need to satisfy

$$C_3^\dagger H(0,0,k_z) C_3 = H(0,0,k_z), \tag{S.14a}$$
$$\sigma_v{}^\dagger H(0,0,k_z) \sigma_v = H(0,0,k_z), \tag{S.14b}$$

where C_3 and σ_v are given by

$$C_3 = \mathrm{diag}(e^{-i\frac{2\pi}{3} j_z}, e^{i\frac{2\pi}{3} j_z}), \tag{S.15a}$$
$$\sigma_v = i s_x, \tag{S.15b}$$

From Eqs. (S.13) and (S.14), the enhancement of rotation symmetry occurs only if the symmetry constraints (S.14) demand $a_x = a_y = 0$. In such a case, we achieve $[H(0,0,k_z), s_z] = 0$, so the Hamiltonian hosts $C_{\infty \mathrm{v}}$ symmetry on the k_z axis, where C_3 is extended to C_∞ such that

$$C_\infty^\dagger H(0,0,k_z) C_\infty = H(0,0,k_z), \tag{S.16}$$

with $C_\infty = \mathrm{diag}(e^{-i\theta j_z}, e^{i\theta j_z})$ $(0 \le \theta < 2\pi)$. Note that the similar argument is applicable to the case without σ_v. In the following, we consider the symmetry constraints for $j_z = 1/2$ and $3/2$.

When $j_z = 1/2$, Eqs. (S.15) are recast into

$$C_3 = e^{-i\frac{\pi}{3}s_z} \tag{S.17a}$$

$$\sigma_v = i s_x. \tag{S.17b}$$

Using Eqs. (S.13) and (S.17), we readily find that Eqs. (S.14) are satisfied only when $a_x = a_y = a_z = 0$; namely, the enhancement is inevitable for spin-1/2.

On the other hand, when $j_z = 3/2$, Eqs. (S.15) are recast into

$$C_3 = -s_0 \tag{S.18a}$$

$$\sigma_v = i s_x. \tag{S.18b}$$

Using Eqs. (S.13) and (S.18), an effective Hamiltonian satisfying Eqs. (S.14) is constructed as

$$H(0,0,k_z) = a_0(k_z) s_0 + b k_z s_x, \tag{S.19}$$

where b is a real coefficient. Therefore, the enhancement does not occur for spin-3/2.

S4. Two-orbital model with magnetic octupole response

Here we present a two-orbital model with magnetic octupole response. Being different from the two-orbital system in S2, the present system consists of p_x and p_y-orbitals, which host $l_z = \pm 1$ angular momenta in the z-direction. Therefore, it contains high spin electrons with $|J_z| = 3/2$. The Hamiltonian in the normal state is given by

$$H(\boldsymbol{k}) = C(\boldsymbol{k})\sigma_0 s_0 + \lambda_1 \sigma_y s_z + \lambda_2 \sin k_z (\sigma_x s_x + \sigma_z s_y), \tag{S.20}$$

where $C(\boldsymbol{k}) = c_0 + t_{xy}\Big\{ \cos k_x + \cos\left(-\frac{1}{2}k_x + \frac{\sqrt{3}}{2}k_y\right) + \cos\left(-\frac{1}{2}k_x - \frac{\sqrt{3}}{2}k_y\right) \Big\} + t_z \cos k_z$, and λ_i $(i = 1, 2)$ are the spin-orbit couplings. Here, σ_i and s_i describe the Pauli matrices in orbital and spin spaces. $\sigma_z = 1$ $(\sigma_z = -1)$ represents the p_x-orbital (p_y-orbital). We assume D_{3h} symmetry, which is generated by

$$\sigma_v = -i\sigma_z s_y, \tag{S.21}$$

$$\sigma_h = -i\sigma_0 s_z, \tag{S.22}$$

$$C_3 = \begin{pmatrix} -\frac{1}{2} & -\frac{\sqrt{3}}{2} \\ \frac{\sqrt{3}}{2} & -\frac{1}{2} \end{pmatrix}_\sigma \otimes e^{-i\frac{\pi}{3}s_z}, \tag{S.23}$$

where σ_v (σ_h) is the mirror-reflection operators with respect to the zx (xy) plane, and C_3 the three-fold rotation operator around the k_z-axis.

We consider the superconducting state which is described by the BdG Hamiltonian

$$\mathcal{H}(\boldsymbol{k}) = \begin{pmatrix} H(\boldsymbol{k}) - \mu & \Delta(\boldsymbol{k}) \\ \Delta(\boldsymbol{k})^\dagger & -H(\boldsymbol{k})^t + \mu \end{pmatrix}, \tag{S.24}$$

with the gap function $\Delta(\boldsymbol{k})$

$$\Delta(\boldsymbol{k}) = i\Delta_0 s_y + \Delta_1 \sigma_y s_x + \Delta_2 \sin k_z (-\sigma_x s_z + i s_0 \sigma_z). \tag{S.25}$$

Here Δ_0, Δ_1, and Δ_2 are constants, and the gap function belongs to the A_1' IR of D_{3h}. The model has three bands described by $E_1(\boldsymbol{k}) = C(\boldsymbol{k}) - \lambda_1$, $E_2(\boldsymbol{k}) = C(\boldsymbol{k}) + \lambda_1 + 2\lambda_2 \sin k_z$, and $E_3(\boldsymbol{k}) = C(\boldsymbol{k}) + \lambda_1 - 2\lambda_2 \sin k_z$, where only the E_1 band is doubly degenerate. Below we consider the case where Δ_2 is dominant and the chemical potential μ lies on

TABLE S1. Possible matrices $O = s_\mu \sigma_\nu$ for local operators of the two-orbital model in S4. We classify O by IRs of D_{3h}.

IR of D_{3h}	TR-even	TR-odd	basis by magnetic fields
A_1'	$\sigma_0 s_0, \sigma_y s_z$		
A_2'		$\sigma_0 s_z, \sigma_y s_0$	B_z
E'	$\{\sigma_x s_0, \sigma_z s_0\}$	$\{\sigma_x s_z, \sigma_z s_z\}$	
A_1''		$\sigma_z s_x - \sigma_x s_y$	$B_x^3 - 3B_x B_y^2$
A_2''		$\sigma_z s_y + \sigma_x s_x$	$B_y^3 - 3B_y B_x^2$
E''	$\{\sigma_y s_x, \sigma_y s_y\}$	$\{\sigma_0 s_x, \sigma_0 s_y\}, \{\sigma_z s_x + \sigma_x s_y, \sigma_x s_x - \sigma_z s_y\}$	$\{B_x, B_y\}$

E_2 and E_3 bands. In this case, the (001) surface hosts a helical MF with flat band associated with the line node at $k_z = 0$. The A_1' pairing symmetry becomes A_1 for the surface point group C_{3v}. For the BdG Hamiltonian, the D_{3h} point group operations are given by

$$\begin{aligned}
\tilde{\sigma}_v &= \mathrm{diag}(\sigma_v, \sigma_v^*) = -i\sigma_x s_y \tau_0, \\
\tilde{\sigma}_h &= \mathrm{diag}(\sigma_h, \sigma_h^*) = -i\sigma_0 s_z \tau_z, \\
\tilde{C}_3 &= \mathrm{diag}(C_3, C_3^*),
\end{aligned} \tag{S.26}$$

where τ_μ are the Pauli matrices in the Nambu space.

In the following, we examine magnetic responses of the helical MF. In the above situation, the following magnetic 1D winding number becomes 2.

$$W(\Gamma_\sigma) = \frac{i}{4\pi} \int_{-\pi}^{\pi} dk_z \ \mathrm{Tr}\left[\Gamma_\sigma \mathcal{H}(\boldsymbol{k})^{-1} \partial_{k_z} \mathcal{H}(\boldsymbol{k})\right] |_{k_x = k_y = 0}, \tag{S.27}$$

with $\Gamma_\sigma = \tilde{\sigma}_v \mathcal{T}\mathcal{C} = s_0 \sigma_z \tau_x$. The corresponding (Kramers) pair of zero modes $|u_0^{(a)}\rangle$ $(a = 1, 2)$ form a helical MF. From the index theorem, the zero modes satisfy $\Gamma_\sigma |u_0^{(a)}\rangle = |u_0^{(a)}\rangle$, and thus they are given by

$$|u_0^{(1)}\rangle = \begin{pmatrix} \begin{pmatrix} \alpha \\ \beta \end{pmatrix}_\sigma \\ \begin{pmatrix} \alpha \\ -\beta \end{pmatrix}_\sigma \end{pmatrix}_\tau \otimes u_s, \quad |u_0^{(2)}\rangle = \mathcal{T}|u_0^{(1)}\rangle, \tag{S.28}$$

where α and β are real coefficients and u_s is an arbitrary function in the spin space. We also have a constraint from C_3 symmetry: From C_3 symmetry, we obtain two additional magnetic chiral operators, $\tilde{C}_3^{-1}\Gamma_\sigma \tilde{C}_3$ and $\tilde{C}_3^{-2}\Gamma_\sigma \tilde{C}_3^2$. They define two additional 1D winding numbers, $W(\tilde{C}_3^{-1}\Gamma_{\sigma_v}\tilde{C}_3)$ and $W(\tilde{C}_3^{-2}\Gamma_{\sigma_v}\tilde{C}_3^2)$, which are equal to $W(\Gamma_\sigma) = 2$. The index theorem tells us again that $\tilde{C}_3^{-1}\Gamma_\sigma \tilde{C}_3 |u_0^{(a)}\rangle = |u_0^{(a)}\rangle$ and $\tilde{C}_3^{-2}\Gamma_\sigma \tilde{C}_3^2 |u_0^{(a)}\rangle = |u_0^{(a)}\rangle$, which are recast into $\Gamma_\sigma \tilde{C}_3 |u_0^{(a)}\rangle = \tilde{C}_3 |u_0^{(a)}\rangle$ and $\Gamma_\sigma \tilde{C}_3^2 |u_0^{(a)}\rangle = \tilde{C}_3^2 |u_0^{(a)}\rangle$. In other words, $|u_0^{(a)}\rangle$, $\tilde{C}_3|u_0^{(a)}\rangle$ and $\tilde{C}_3^2|u_0^{(a)}\rangle$ are eigenstates of Γ_σ with the same eigenvalue $\Gamma_\sigma = 1$. Moreover, we can obtain an eigenstate of $\tilde{C}_3$ by combining these states. Therefore, the zero modes can be simultaneous eigenstates of Γ_σ and $\tilde{C}_3$. Since Γ_σ and $\tilde{C}_3$ obey $\Gamma_\sigma \tilde{C}_3 \Gamma_\sigma = \tilde{C}_3^{-1}$, the eigenvalue of $\tilde{C}_3$ must be -1. Imposing the eigenvalue condition for $\tilde{C}_3$ on Eq. (S.28), we obtain

$$|u_0^{(1)}\rangle = \begin{pmatrix} C \\ iC \\ D \\ -iD \\ C \\ -iC \\ D \\ iD \end{pmatrix}, \quad |u_0^{(2)}\rangle = \mathcal{T}|u_0^{(1)}\rangle, \tag{S.29}$$

where C and D are real coefficients, and we take the Nambu space as $(\hat{c}_{1\uparrow}, \hat{c}_{1\downarrow}, \hat{c}_{2\uparrow}, \hat{c}_{2\downarrow}, \hat{c}_{1\uparrow}^\dagger, \hat{c}_{1\downarrow}^\dagger, \hat{c}_{2\uparrow}^\dagger, \hat{c}_{2\downarrow}^\dagger)^t$ with the spin $s = (\uparrow, \downarrow)$ and the orbital $\sigma = (1, 2)$.

Now we perform the mode expansion of the quantum field

$$\mathbf{\Psi}(x) = \begin{pmatrix} \hat{c}_{1s}(x) \\ \hat{c}_{2s}(x) \\ \hat{c}_{1s}(x)^\dagger \\ \hat{c}_{2s}(x)^\dagger \end{pmatrix} = \sum_{a=1,2} |u_0^{(a)}\rangle \hat{\gamma}^{(a)} + (\text{non-zero energy mode}). \tag{S.30}$$

Neglecting the non-zero energy modes, we find

$$\hat{c}_{1s} = \hat{c}_{1s}^\dagger, \quad \hat{c}_{2s} = -\hat{c}_{2s}^\dagger. \tag{S.31}$$

$$\hat{c}_{2\uparrow} = i\hat{c}_{1\uparrow} = -\hat{c}_{2\uparrow}^\dagger = i\hat{c}_{1\uparrow}^\dagger, \quad \hat{c}_{2\downarrow} = -i\hat{c}_{1\downarrow} = -\hat{c}_{2\downarrow}^\dagger = -i\hat{c}_{1\downarrow}^\dagger. \tag{S.32}$$

from Eqs.(S.28) and (S.29).

Using these relations, we find that the local density and spin density operators of the zero modes vanish such that

$$\begin{aligned}
\hat{\rho}_{\rm MF} &= \frac{1}{2}\mathbf{\Psi}(x)^\dagger \,\mathrm{diag}(s_0\sigma_0, -s_0\sigma_0)\mathbf{\Psi}(x)|_{\rm MF} \\
&= \frac{1}{2}\left(c_{1s}^\dagger c_{1s} + c_{2s}^\dagger c_{2s} - c_{1s}c_{1s}^\dagger - c_{2s}c_{2s}^\dagger\right) \\
&= \frac{1}{2}\left(c_{1s}^\dagger c_{1s}^\dagger - c_{2s}^\dagger c_{2s}^\dagger - c_{1s}^\dagger c_{1s}^\dagger + c_{2s}^\dagger c_{2s}^\dagger\right) \\
&= 0. \\
(\hat{S}_{i=x,z})_{\rm MF} &= \frac{1}{4}\mathbf{\Psi}(x)^\dagger \,\mathrm{diag}(s_i\sigma_0, -s_i\sigma_0)\mathbf{\Psi}(x)|_{\rm MF} \\
&= \frac{1}{4}(c_{1s}^\dagger (s_i)_{ss'} c_{1s'} + c_{2s}^\dagger (s_i)_{ss'} c_{2s'} - c_{1s}(s_i^t)_{ss'} c_{1s'}^\dagger - c_{2s}(s_i^t)_{ss'} c_{2s'}^\dagger) \\
&= \frac{1}{4}(c_{1s}^\dagger (s_i)_{ss'} c_{1s'}^\dagger - c_{2s}^\dagger (s_i)_{ss'} c_{2s'}^\dagger - c_{1s}^\dagger (s_i^t)_{ss'} c_{1s'}^\dagger + c_{2s}^\dagger (s_i^t)_{ss'} c_{2s'}^\dagger) \\
&= 0. \\
(\hat{S}_y)_{\rm MF} &= \frac{1}{4}\mathbf{\Psi}(x)^\dagger \,\mathrm{diag}(s_y\sigma_0, s_y\sigma_0)\mathbf{\Psi}(x)|_{\rm MF} \\
&= \frac{1}{2}\left(\hat{c}_{1s}^\dagger (s_y)_{ss'} \hat{c}_{1s'}^\dagger - \hat{c}_{2s}^\dagger (s_y)_{ss'} \hat{c}_{2s'}^\dagger\right) \\
&= \frac{1}{2}\left(-i\hat{c}_{1\uparrow}^\dagger \hat{c}_{1\downarrow}^\dagger + i\hat{c}_{1\downarrow}^\dagger \hat{c}_{1\uparrow}^\dagger + i\hat{c}_{2\uparrow}^\dagger \hat{c}_{2\downarrow}^\dagger - i\hat{c}_{2\downarrow}^\dagger \hat{c}_{2\uparrow}^\dagger\right) \\
&= \frac{1}{2}\left(-i\hat{c}_{1\uparrow}^\dagger \hat{c}_{1\downarrow}^\dagger + i\hat{c}_{1\downarrow}^\dagger \hat{c}_{1\uparrow}^\dagger + i(-i)\hat{c}_{1\uparrow}^\dagger i\hat{c}_{1\downarrow}^\dagger - ii\hat{c}_{1\downarrow}^\dagger (-i)\hat{c}_{1\uparrow}^\dagger\right) \\
&= 0
\end{aligned} \tag{S.33, S.34}$$

We can also evaluate other orbital-dependent operators $\sigma_i s_j$ in Table S1. For instance, $\mathcal{O}_1 = \mathrm{diag}(\sigma_y s_y, -\sigma_y s_y)$,

$\mathcal{O}_2 = \mathrm{diag}(\sigma_z s_y + \sigma_x s_x, \sigma_z s_y - \sigma_x s_x)$, and $\mathcal{O}_3 = \mathrm{diag}(\sigma_z s_y - \sigma_x s_x, \sigma_z s_y + \sigma_x s_x)$ are evaluated as

$$\begin{aligned}
(\hat{\mathcal{O}}_1)_{\mathrm{MF}} &= \frac{i}{2}\left(c^\dagger_{1s}(s_y)_{ss'}c^\dagger_{2s} + c^\dagger_{2s}(s_y)_{ss'}c^\dagger_{1s}\right)\\
&= \frac{i}{2}\left(-ic^\dagger_{1\uparrow}c^\dagger_{2\downarrow} + ic^\dagger_{1\downarrow}c^\dagger_{2\uparrow} - ic^\dagger_{2\uparrow}c^\dagger_{1\downarrow} + ic^\dagger_{2\downarrow}c^\dagger_{1\uparrow}\right)\\
&= \frac{i}{2}\left(-ic^\dagger_{1\uparrow}c^\dagger_{2\downarrow} + ic^\dagger_{1\downarrow}c^\dagger_{2\uparrow} - i(-i)c^\dagger_{1\uparrow}(-i)c^\dagger_{2\downarrow} + iic^\dagger_{1\downarrow}ic^\dagger_{2\uparrow}\right)\\
&= 0,\\
(\hat{\mathcal{O}}_2)_{\mathrm{MF}} &= \frac{1}{2}\left[\left(\hat{c}^\dagger_{1s}(s_y)_{ss'}\hat{c}^\dagger_{1s'} + \hat{c}^\dagger_{2s}(s_y)_{ss'}\hat{c}^\dagger_{2s'}\right) + \left(-\hat{c}^\dagger_{1s}(s_x)_{ss'}\hat{c}^\dagger_{2s'} + \hat{c}^\dagger_{2s}(s_x)_{ss'}\hat{c}^\dagger_{1s'}\right)\right]\\
&= \left[\left(-i\hat{c}^\dagger_{1\uparrow}\hat{c}^\dagger_{1\downarrow} + i\hat{c}^\dagger_{1\downarrow}\hat{c}^\dagger_{1\uparrow}\right) + \left(-\hat{c}^\dagger_{1\uparrow}\hat{c}^\dagger_{2\downarrow} - \hat{c}^\dagger_{1\downarrow}\hat{c}^\dagger_{2\uparrow}\right)\right]\\
&= \left[\left(-i\hat{c}^\dagger_{1\uparrow}\hat{c}^\dagger_{1\downarrow} + i\hat{c}^\dagger_{1\downarrow}\hat{c}^\dagger_{1\uparrow}\right) + \left(-i\hat{c}^\dagger_{1\uparrow}\hat{c}^\dagger_{1\downarrow} + i\hat{c}^\dagger_{1\downarrow}\hat{c}^\dagger_{1\uparrow}\right)\right]\\
&\neq 0,\\
(\hat{\mathcal{O}}_3)_{\mathrm{MF}} &= \frac{1}{2}\left[\left(\hat{c}^\dagger_{1s}(s_y)_{ss'}\hat{c}^\dagger_{1s'} + \hat{c}^\dagger_{2s}(s_y)_{ss'}\hat{c}^\dagger_{2s'}\right) - \left(-\hat{c}^\dagger_{1s}(s_x)_{ss'}\hat{c}^\dagger_{2s'} + \hat{c}^\dagger_{2s}(s_x)_{ss'}\hat{c}^\dagger_{1s'}\right)\right]\\
&= \left[\left(-i\hat{c}^\dagger_{1\uparrow}\hat{c}^\dagger_{1\downarrow} + i\hat{c}^\dagger_{1\downarrow}\hat{c}^\dagger_{1\uparrow}\right) - \left(-\hat{c}^\dagger_{1\uparrow}\hat{c}^\dagger_{2\downarrow} - \hat{c}^\dagger_{1\downarrow}\hat{c}^\dagger_{2\uparrow}\right)\right]\\
&= \left[\left(-i\hat{c}^\dagger_{1\uparrow}\hat{c}^\dagger_{1\downarrow} + i\hat{c}^\dagger_{1\downarrow}\hat{c}^\dagger_{1\uparrow}\right) - \left(-i\hat{c}^\dagger_{1\uparrow}\hat{c}^\dagger_{1\downarrow} + i\hat{c}^\dagger_{1\downarrow}\hat{c}^\dagger_{1\uparrow}\right)\right]\\
&= 0.
\end{aligned} \tag{S.35}$$

Actually, we find that only $(\hat{\mathcal{O}}_2)_{\mathrm{MF}}$ do not vanish among all possible local operators. Note that $(\hat{\mathcal{O}}_2)_{\mathrm{MF}}$ is odd under TR and belongs to the A_2'' IR of D_{3h}, and $B_y^3 - 3B_yB_x^2$ has the same symmetry properties. Thus, the lowest order coupling between the MF and magnetic feilds is $(\hat{\mathcal{O}}_2)_{\mathrm{MF}}(B_y^3 - 3B_yB_x^2)$, which gives a magnetic octupole response.

S5. Topological surface states of the A_1 state in half-Heusler superconductors

We start with the BdG Hamiltonian of the spin-3/2 half-Heusler superconductor [42]

$$\mathcal{H}(\boldsymbol{k}) = \begin{pmatrix} H_{\mathrm{LK}}(\boldsymbol{k}) - \mu & \Delta(\boldsymbol{k}) \\ \Delta(\boldsymbol{k})^\dagger & -H_{\mathrm{LK}}(-\boldsymbol{k})^t + \mu \end{pmatrix}, \tag{S.36}$$

with

$$H_{\mathrm{LK}}(\boldsymbol{k}) = \alpha\boldsymbol{k}^2 + \beta\sum_i k_i J_i^2 + \gamma\sum_{i\neq j} k_i k_j J_i J_j + \delta\sum_i k_i(J_{i+1}J_iJ_{i+1} - J_{i+2}J_iJ_{i+2}), \tag{S.37}$$

$$\Delta(\boldsymbol{k}) = \Delta/\sqrt{1+\eta^2}[\eta 1_4 + \sum_i k_i(J_{i+1}J_iJ_{i+1} - J_{i+2}J_iJ_{i+2})](e^{-iJ_y\pi}). \tag{S.38}$$

Here J_i's are the three spin matrices of 3/2-fermions, described as

$$J_x = \frac{1}{2}\begin{pmatrix} 0 & \sqrt{3} & 0 & 0 \\ \sqrt{3} & 0 & 2 & 0 \\ 0 & 2 & 0 & \sqrt{3} \\ 0 & 0 & \sqrt{3} & 0 \end{pmatrix}, \quad J_y = \frac{i}{2}\begin{pmatrix} 0 & -\sqrt{3} & 0 & 0 \\ \sqrt{3} & 0 & -2 & 0 \\ 0 & 2 & 0 & -\sqrt{3} \\ 0 & 0 & \sqrt{3} & 0 \end{pmatrix}, \quad J_z = \frac{1}{2}\begin{pmatrix} 3 & 0 & 0 & 0 \\ 0 & 1 & 0 & 0 \\ 0 & 0 & -1 & 0 \\ 0 & 0 & 0 & -3 \end{pmatrix}. \tag{S.39}$$

The spin-orbit interactions (SOIs) proportional to β and γ are inversion symmetric, while the δ term is odd under inversion, describing an anti-symmetric SOI. The band spectrum of the normal Hamiltonian $H_{\mathrm{LK}}(\boldsymbol{k})$ shows four-fold degeneracy of $J = 3/2$ at the Γ point. Apart from the Γ point, the energy dispersion splits into two doubly degenerate bands when $\delta = 0$. When the δ term is turned on, its degeneracy splits due to the breaking of inversion symmetry. PH and TR operations for the BdG Hamiltonian are $\mathcal{C} = \tau_x K$ and $\mathcal{T} = e^{-iJ_y\pi}K$, respectively, and T_d for the BdG Hamiltonian is generated by rotations $\mathcal{U}_{q,\boldsymbol{n}} = \mathrm{diag}[e^{i\frac{i2\pi}{q}\boldsymbol{J}\cdot\boldsymbol{n}}, e^{-i\frac{i2\pi}{q}\boldsymbol{J}^*\cdot\boldsymbol{n}}]$ and mirror reflections $\tilde{\sigma} = \mathrm{diag}[\sigma, \sigma^*]$ where σ represents diagonal and vertical mirror reflections for the normal Hamiltonian.

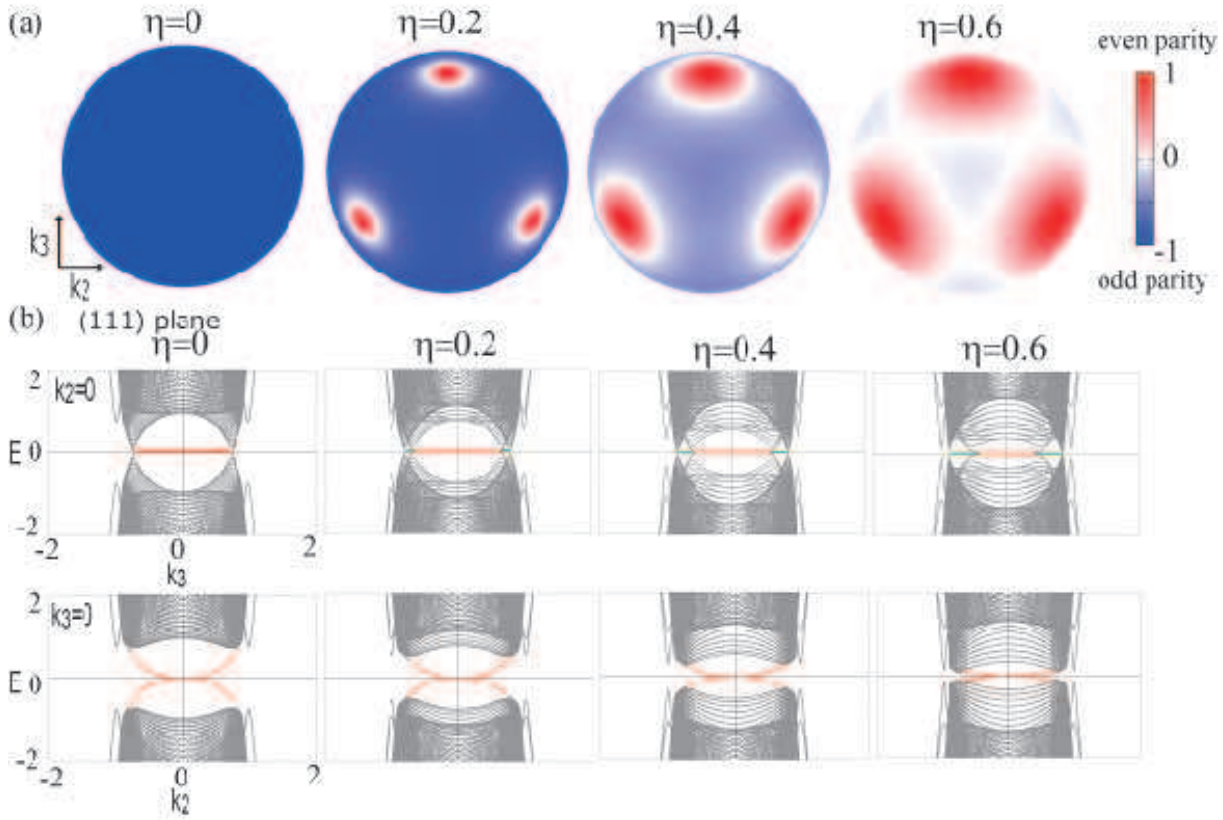


FIG. S2. (a) Node structure in the Hamiltonian (S.36) with parameter $(\alpha, \beta, \gamma, \delta, \mu, \Delta) = (20, -15, -15, 0, -10, 1)$. The color shows $(\psi^2 - |\boldsymbol{d}|^2)/(\psi^2 + |\boldsymbol{d}|^2)$, where ψ and $\boldsymbol{d}$ describes spin-singlet and pseudospin-triplet components on the basis projected into the spin 3/2 band [42]. The point nodes inflate into the line nodes depicted by the while lines in an increase in η. (b) Surface energy spectrum along the $k_3 = \boldsymbol{k} \cdot \boldsymbol{n}_3$ (the top panels) and the $k_2 = \boldsymbol{k} \cdot \boldsymbol{n}_2$ axes (the bottom panels), where $\boldsymbol{n}_2 = \frac{1}{\sqrt{2}}(1, -1, 0)$ and $\boldsymbol{n}_3 = \frac{1}{\sqrt{6}}(1, 1, -2)$. The red and green lines exhibit the Majorana arc state terminating at a pair of point nodes and the Majorana flat band coming from the line nodes, respectively. For a small η, the helical MF located at $k_2 = k_3 = 0$ still survives.

In Fig. S2 (a), we show the node structure of the superconducting state on the spherical Fermi surface. When $\eta = 0$, $\Delta(\boldsymbol{k})$ is the pure septet pairing and hosts point nodes on the x, y, and z axes. For a small η, the mixture of spin-singlet and spin-septet components inflates point nodes to line nodes in a similar way to other non-centrosymmetric SCs [65]. Crucially, in the [111] direction, the spin-septet component is most dominant on the Fermi surface. In Fig. S2 (b), we show topological surface states of the system, which are calculated by replacing k_i, k_i^2 with $\sin k_i, 2(1 - \cos k_i)$ and imposing the open boundary condition along the [111] direction. The obtained surface energy spectra are shown. When $\eta = 0$, the pure spin-septet superconductor hosts six point nodes, which induce the Majorana arc state in the k_3 direction, which connects projected point nodes on the surface BZ. Adding the spin-singlet component ($\eta \neq 0$), line nodes arise and induce non-degenerate surface flat bands. See the top panel of Fig. S2 (b). Despite the mixing of the spin-singlet component, the helical MF located at $\boldsymbol{k}_\parallel = 0$ is stable when $\eta < \eta_c \simeq 0.9$. The similar topological surface states are obtained when $\beta \neq \gamma$ and $\delta \neq 0$. For Fig. 2 in the main paragraph, we take the parameters as $(\alpha, \beta, \gamma, \delta, \mu, \Delta, \eta) = (20, -15, -10, 1, -10, 0.5, 0.2)$, where we have confirmed the presence of the Majorana arc states and the non-degenerate surface flat bands on the (111) surface.

The existence of the Majorana arc states is ensured by the magnetic 1D winding number

$$W(\boldsymbol{k}_\parallel, \Gamma_\sigma) \equiv \frac{i}{4\pi} \int_{-\pi}^{\pi} dk_\perp \ \mathrm{Tr}\left[\Gamma_\sigma \mathcal{H}(\boldsymbol{k})^{-1} \partial_{k_\perp} \mathcal{H}(\boldsymbol{k})\right], \tag{S.40}$$

where $\Gamma_\sigma = \tilde{\sigma}\mathcal{T}\mathcal{C}$ with $\tilde{\sigma}$ the diagoal mirror reflection. Here $(\boldsymbol{k}_\parallel, k_\perp)$ are the momentum parallel to and normal to the surface, respectively, and $\boldsymbol{k}_\parallel$ in the left hand side of Eq.(S.40) should be on the diagonal mirror plane, say $\boldsymbol{k}_\parallel = (0, k_3)$. Because of C_3 symmetry of the surface, we have Majorana arcs on three equivalent directions. In

particular, the three Majorana arcs form a single distorted helical MF with C_{3v} symmetry centered $\boldsymbol{k}_\parallel = 0$. When $\eta \neq 0$, the mixture between the spin-singlet and spin-septet components gives rise to line nodes, as mentioned in the above. The line nodes host the 1D winding number $W(\boldsymbol{k}_\parallel, \Gamma)$ of the conventional chiral operator $\Gamma = -i\mathcal{T}\mathcal{C}$ [58], and thus the non-degenerate flat bands mentioned above appear. We emphasize here that the Majorana arc states by $W(\boldsymbol{k}_\parallel, \Gamma_\sigma)$ and non-degenerate flat bands by $W(\boldsymbol{k}_\parallel, \Gamma)$ coexist and the helical MF survives as long as $\eta < \eta_c$, where η_c is a topological phase transition point with respect to $W(\boldsymbol{k}_\parallel = 0, \Gamma_\sigma)$.

S6. Energy gap and magnetic octupole response

To see the magnitude of the energy gap for the helical MF under the magnetic octupole response, we consider Eq. (S.37) with the Zeeman magnetic field: $H_{LK}(\boldsymbol{k}) + \mu \boldsymbol{B} \cdot \boldsymbol{J}$. On the basis that diagonalizes $H_{\rm LK}(\boldsymbol{k})$ with $\delta = \mu = 0$, the Hamiltonian on the [111] direction becomes

$$U^\dagger H_{\rm LK}(k) U = \frac{k^2}{4} \,\mathrm{diag}[4\alpha + 5\beta + 4\gamma, 4\alpha + 5\beta + 4\gamma, 4\alpha + 5\beta - 4\gamma, 4\alpha + 5\beta - 4\gamma], \tag{S.41}$$

with

$$U = \frac{e^{i\frac{\pi}{4}}}{\sqrt{6}} \begin{pmatrix} -1-i & -i & 0 & \sqrt{3} \\ -i\sqrt{3} & 0 & 1 & -1-i \\ 0 & \sqrt{3} & -1-i & -i \\ 1 & -1-i & -i\sqrt{3} & 0 \end{pmatrix}. \tag{S.42}$$

The TR operator and the C_{3v} symmetry operator are also given by

$$U^\dagger e^{-iJ_y\pi} U^* = \begin{pmatrix} 0 & 1 & 0 & 0 \\ -1 & 0 & 0 & 0 \\ 0 & 0 & 0 & 1 \\ 0 & 0 & -1 & 0 \end{pmatrix}, \tag{S.43}$$

$$U^\dagger e^{-i\frac{J_x+J_y+J_z}{\sqrt{3}}\frac{2\pi}{3}} U = \begin{pmatrix} -1 & 0 & 0 & 0 \\ 0 & -1 & 0 & 0 \\ 0 & 0 & \frac{1+i}{2} & \frac{1-i}{2} \\ 0 & 0 & -\frac{1+i}{2} & \frac{1-i}{2} \end{pmatrix}, \tag{S.44}$$

$$U^\dagger e^{-i\frac{J_x-J_y}{\sqrt{2}}\pi} U = \begin{pmatrix} 0 & -e^{i\frac{\pi}{4}} & 0 & 0 \\ -e^{i\frac{3\pi}{4}} & 0 & 0 & 0 \\ 0 & 0 & 0 & e^{i\frac{\pi}{4}} \\ 0 & 0 & e^{i\frac{3\pi}{4}} & 0 \end{pmatrix}. \tag{S.45}$$

Projecting the Hamiltonian into the spin-3/2 band and including the anti-symmetry SOI and the magnetic Zeeman term as a perturbation up to the third order, Eqs. (S.41), (S.43), (S.44), and (S.45) are given by

$$\begin{aligned} H_{\rm eff}(k) &= \frac{k^2}{4}(4\alpha + 5\beta + 4\gamma)\sigma_0 - \frac{\sqrt{3}k}{2}\delta(\sigma_x + \sigma_y) + \frac{\sqrt{3}}{2}\mu B_1(\sigma_x + \sigma_y + \sigma_z) \\ &+ \frac{3}{2\Delta\epsilon(k)}\mu^2(B_2^2 + B_3^2)\sigma_0 + \frac{\sqrt{3}}{8\Delta\epsilon(k)^2}\mu^3\Big[\Big\{-2B_1(B_2^2 + B_3^2) + 2\sqrt{2}B_3(B_3^2 - 3B_2^2)\Big\}\sigma_z \\ &- \Big\{2B_1(B_2^2 + B_3^2) + \sqrt{2}B_3(B_3^2 - 3B_2^2) + \sqrt{3}B_2(B_2^2 - 3B_3^2)\Big\}\sigma_x \\ &- \Big\{2B_1(B_2^2 + B_3^2) + \sqrt{2}B_3(B_3^2 - 3B_2^2) - \sqrt{3}B_2(B_2^2 - 3B_3^2)\Big\}\sigma_y\Big], \end{aligned} \tag{S.46}$$

$$T_{\rm eff} = i\sigma_y K, \tag{S.47}$$

$$U_{3,\rm eff} = -\sigma_0, \tag{S.48}$$

$$U_{\sigma_v,\rm eff} = \frac{i}{\sqrt{2}}(\sigma_x - \sigma_y). \tag{S.49}$$

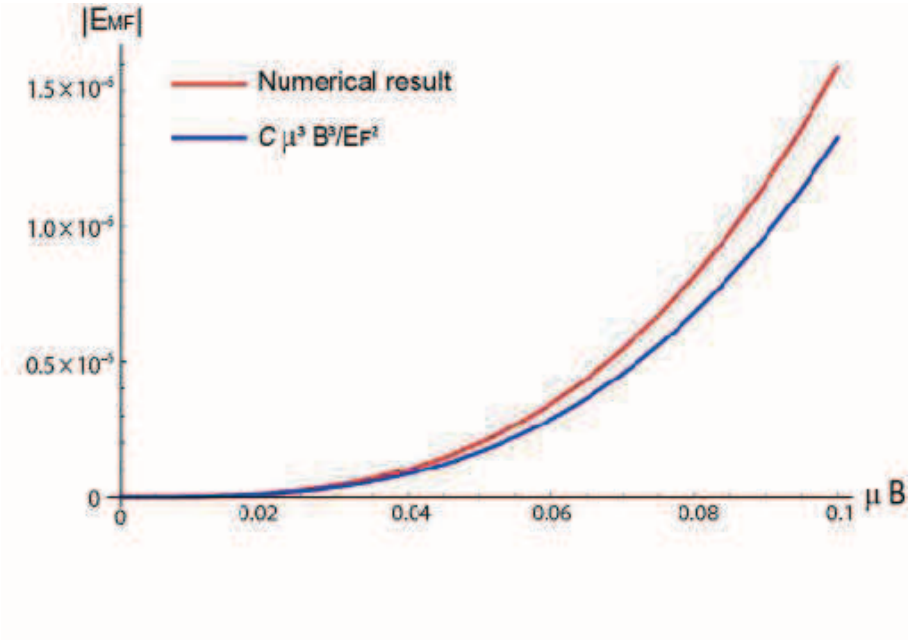


FIG. S3. The magnitude of the energy gap $E_{\rm MF}$ as a function of B. The red thick and blue thick lines represent the numerical and analytical results, respectively, where $C = 3\sqrt{2}/32$. The parameters and the direction of the Zeeman magnetic field are chosen as $(\alpha, \beta, \gamma, \delta, \mu, \Delta, \eta) = (20, -15, -15, 0, -10, 1, 0)$ and $(\theta, \phi) = (\pi/2, 0)$, respectively.

where $(\sigma_0, \boldsymbol{\sigma})$ are the 2×2 identity matrix and the Pauli matrices, $\Delta\epsilon(k) \equiv \epsilon_{3/2}(k) - \epsilon_{1/2}(k)$, and $(B_1, B_2, B_3) \equiv (\frac{1}{\sqrt{3}}\{B_x + B_y + B_z\}, \frac{1}{\sqrt{2}}\{B_x - B_y\}, \frac{1}{\sqrt{6}}\{B_x + B_y - 2B_z\})$. Introducing $\sigma_1 \equiv \frac{1}{\sqrt{3}}(\sigma_x + \sigma_y + \sigma_z)$, $\sigma_2 \equiv \frac{1}{\sqrt{2}}(\sigma_x - \sigma_y)$, and $\sigma_3 \equiv \frac{1}{\sqrt{6}}(\sigma_x + \sigma_y - 2\sigma_z)$, Eq. (S.46) is recast into

$$\begin{aligned} H_{\rm eff}(k) = {} & \frac{k^2}{4}(4\alpha + 5\beta + 4\gamma)\sigma_0 - k\delta\left(\sigma_1 + \frac{1}{\sqrt{2}}\sigma_3\right) + \frac{3}{2}\mu B_1\sigma_1 + \frac{3}{2\Delta\epsilon(k)}\mu^2(B_2^2 + B_3^2)\sigma_0 \\ & - \frac{3}{4\Delta\epsilon(k)^2}\mu^3\Big[B_1(B_2^2 + B_3^2)\sigma_1 + \frac{1}{\sqrt{2}}B_2(B_2^2 - 3B_3^2)\sigma_2 + B_3(B_3^2 - 3B_2^2)\sigma_3\Big]. \end{aligned} \tag{S.50}$$

Within the effective Hamiltonian, the BdG Hamiltonian is given by

$$\mathcal{H}_{\rm eff}(k) = \begin{pmatrix} H_{\rm eff}(k) - E_{\rm F}\sigma_0 & \Delta(k) \\ \Delta(k)^\dagger & -H_{\rm eff}(-k)^t + E_{\rm F}\sigma_0 \end{pmatrix}, \tag{S.51}$$

with the Fermi energy $E_{\rm F}$ and the gap function $\Delta(k) = \frac{\Delta}{\sqrt{1+\eta^2}}\left\{\eta\sigma_0 - \frac{\sqrt{3}k}{2}(\sigma_x + \sigma_y)\right\} i\sigma_y$. In addition, Eqs. (S.47), (S.48), and (S.49) are extended into the Nambu space:

$$\mathcal{T}_{\rm eff} = i\sigma_y\tau_0 K, \tag{S.52}$$

$$\mathcal{U}_{3,\rm eff} = -\sigma_0\tau_0, \tag{S.53}$$

$$\mathcal{U}_{\sigma,\rm eff} = \frac{i}{\sqrt{2}}(\sigma_x\tau_z - \sigma_y\tau_0), \tag{S.54}$$

where $(\tau_0, \boldsymbol{\tau})$ are the 2×2 identity matrix and the Pauli matrices describing the Nambu space. The BdG Hamiltonian hosts the magnetic chiral symmetry $\{\mathcal{H}_{\rm eff}(k), \Gamma_\sigma\} = 0$ with $\Gamma_\sigma \equiv \mathcal{U}_{\sigma_v,\rm eff}\mathcal{T}_{\rm eff}\mathcal{C}$, which involves a nonzero 1D winding number and ensures the MF on the surface. Here $\mathcal{C} = \tau_x K$ is the PH operator. Furthermore, due to the C_3 symmetry, we have different magnetic chiral operators: $\mathcal{U}_{3,\rm eff}^\dagger\Gamma_\sigma\mathcal{U}_{3,\rm eff}$ and $(\mathcal{U}_{3,\rm eff}^\dagger)^2\Gamma_\sigma(\mathcal{U}_{3,\rm eff})^2$, which also protect the MF at the same time. Hence, the corresponding MF can be a quantum state $|u_0^{(a)}\rangle$ $(a = 1, 2)$ that is an simultaneous eigenstate of $\Gamma_\sigma = \frac{1}{\sqrt{2}}(\sigma_z\tau_y + \sigma_0\tau_x)$ and $\mathcal{U}_{3,\rm eff}$, e.g., $\Gamma_\sigma|u_0^{(a)}\rangle = |u_0^{(a)}\rangle$ and $\mathcal{U}_{3,\rm eff}|u_0^{(a)}\rangle = -|u_0^{(a)}\rangle$. Taking the symmetry constraints

into account, we calculate the expectation value $\langle u_0^{(a)}|\tilde{\sigma}_i|u_0^{(b)}\rangle$ with $\tilde{\sigma}_i = \mathrm{diag}[\sigma_i, -\sigma_i^*]$ $(i = 0, 1, 2, 3)$. After algebraic calculations, we find

$$\{\Gamma_{\sigma_v}, \tilde{\sigma}_0\} = \{\Gamma_{\sigma_v}, \tilde{\sigma}_1\} = [\Gamma_{\sigma_v}, \tilde{\sigma}_2] = \{\Gamma_{\sigma_v}, \tilde{\sigma}_3\} = 0, \tag{S.55}$$

so only $\langle u_0^{(a)}|\tilde{\sigma}_2|u_0^{(b)}\rangle$ remains nonzero. The Zeeman magnetic term that affects the MF becomes

$$\langle u_0^{(a)}|\tilde{H}_{\mathrm{eff,Zeeman}}|u_0^{(b)}\rangle = -\frac{3\sqrt{2}}{8\Delta\epsilon(k)^2}\mu^3 B_2(B_2^2 - 3B_3^2)\langle u_0^{(a)}|\tilde{\sigma}_2|u_0^{(b)}\rangle. \tag{S.56}$$

When the spin-3/2 (1/2) band curves oppositely and $\delta \ll 1$, $\Delta\epsilon(k) \sim 2E_{\mathrm{F}}$. Then, the magnitude of the energy gap is estimated as

$$|E_{\mathrm{MF}}| \propto \frac{3\sqrt{2}}{32}\frac{\mu^3 B^3}{E_{\mathrm{F}}^2}\sin^3\theta\cos 3\phi, \tag{S.57}$$

when $(B_1, B_2, B_3) = B(\cos\theta, \sin\theta\cos\phi, \sin\theta\sin\phi)$. The comparison between the analytical and the numerical results are shown in Fig. S3.